

promoting access to White Rose research papers



Universities of Leeds, Sheffield and York
<http://eprints.whiterose.ac.uk/>

This is an author produced version of a paper published in **Journal of Tribology**.

White Rose Research Online URL for this paper:

<http://eprints.whiterose.ac.uk/43103/>

Published paper

Dwyer-Joyce, R.S., Reddyhoff, T. and Zhu, J. (2011) *Ultrasonic Measurement for Film Thickness and Solid Contact in Elastohydrodynamic Lubrication*. *Journal of Tribology*, 133 (3). 031501.

<http://dx.doi.org/10.1115/1.4004105>

Ultrasonic Measurement for Film Thickness and Solid Contact in Elastohydrodynamic Lubrication

R. S. Dwyer-Joyce¹, T. Reddyhoff² and J. Zhu¹

¹ The Leonardo Centre, Department of Mechanical Engineering, University of Sheffield, Sheffield S1 3JD, UK

²Tribology Group, Imperial College, London SW7 2AZ, UK

Abstract

The reflection of ultrasound can be used to determine oil film thickness in elastohydrodynamic lubricated (EHL) contacts if the opposing surfaces are fully separated by the liquid layer. The proportion of the wave amplitude reflected depends on the stiffness of the liquid layer, which is a function of its bulk modulus and thickness. However, in many practical applications, boundary or mixed film lubrication is a common occurrence as the nominal thickness of the separating film is of a similar order to the height of the surface asperities. The reflection is then dependent on both the liquid contact and solid contact parts and the total interfacial stiffness is the controlling parameter.

In this paper an investigation was carried to study the reflection of ultrasonic waves from the lubricated contact between a sliding steel ball and a flat steel disc when substantial solid contact occurs. To interpret the ultrasonic reflection results a mixed regime model for a circular point contact was established. The liquid film stiffness was calculated by using a predicted film thickness and a bulk modulus estimated from published rheological models of lubricants under high pressure. Solid contact stiffness was predicted using a statistical rough surface contact model. Under all operating conditions, the prediction of fluid stiffness was found to be much greater than the solid contact stiffness. The total stiffness predicted by the model showed good agreement with experimental measurements for kinematic cases. The model was used to separate the stiffness contributions from the asperity contact part and lubricant layer part from the experimental data. For a contact pressures ranging from 0.42 to 0.84 GPa and sliding speed from zero to 2 m/s, the film thickness was found to vary from 0.01 to 0.8 μm , and the proportion of the load supported by asperity contact varied from 50% to 0%.

1. Introduction

Ideally machine elements like gears and rolling bearings should be lubricated by thick films that separate the running surfaces. However, frequently the hydrodynamic action is insufficient to generate a fluid film thick enough to separate the asperities. The interface then consists of isolated asperity contacts with the surrounding gaps filled by liquid. The load is shared between direct solid to solid asperity contact and a liquid film. This is known as the regime of mixed lubrication. The exact nature of the solid to solid contact parts is highly complex and may consist of adsorbed molecular species and thin transformed layers [1]. However, for the purposes of this paper we simply distinguish between liquid and solid contact.

In mixed elastohydrodynamic lubrication, the separation between two matching surfaces is of a similar order to the surface roughness. Both asperity contact and lubricant load support exists.

Corresponding author: Juanjuan ZHU, Paper No: TRIB-10-1223, page number 1

The total load on the contact P_T is assumed to be shared by contacting asperities and compressed lubricant. This concept of load sharing relationship $P_T = P_a + P_l$ is widely used for modelling mixed lubrication problems [2, 3 and 4]. Johnson *et al.* [5] introduced the scaling factor γ to define these two parts. In that model, it was assumed that hydrodynamic film formation and solid contact are mutually independent, so that the film formation is not affected by the presence of roughness. A statistical model of rough surface contact was combined with a solution for smooth surface elastohydrodynamic film thickness. A similar approach was adopted by Gelinck & Schipper [6] who combined the relevant solid contact equations and lubrication theory to predict film thickness and friction for line contact problems.

Whilst modelling of mixed lubrication contact has progressed considerably, experimental techniques have not. The lubricant films formed are very thin and asperity contacts very small, so it has proved difficult to obtain direct measurements. Electrical methods have been useful indicators of when asperity contact occurs. The resistance of lubricated contacts reduces by several orders of magnitude when contact occurs. Usually data is expressed as a non-contact time fraction [7], which reduces with surface roughness or increasing film thickness.

In optical interferometry techniques, film thickness is deduced from the interference pattern produced by the interaction of light beams reflecting from the top and bottom surfaces of the oil film. The approach can measure films extremely accurately, and requires no calibration. A spacer layer is incorporated into the optical path to permit the interferometric measurement of films down to a nanometre thickness [8]. This technique has been proved very useful in the study of boundary and mixed lubricant films [9, 10].

The reflection of ultrasound has been used to study rough surface contacts [11-18]. The proportion of the wave reflected depends on the stiffness of the rough surface interface. The measurement of stiffness in this way has been used to study elastic plastic contact [19- 21] and contact non-linearity [22, 23]. The reflection also occurs when the interface consists of a thin layer of liquid. This has been used for the measurement of thin oil films in machine components [24- 27].

In this work, the use of ultrasound to measure mixed liquid and solid contact is explored. Transmission occurs at both asperities contact and fluid layer simultaneously. In parallel, a model of film formation of the mixed lubrication regime has been used and results compared to the ultrasonic response. In this way it has proved possible to separate and deduce the liquid and solid contact in the experimental cases.

2. Ultrasonic response

(a) Dry rough surface contact

The response of a dry contact for an ultrasonic wave (shown schematically in Figure 1(a)) has been studied by a number of workers. Work has been motivated both for its implications on crack detection [28, 29], transmission through structures [30], contact in bearing systems [11], and contact area and pressure distribution in machine elements [31, 32].

When an ultrasonic wave is incident at a rough surface contact between two solids, the proportion of the wave amplitude reflected, known as the reflection coefficient, depends on the conformity between the two bodies. Kendal and Tabor [11] showed that the reflection coefficient, R depends

on the stiffness of the interface, K . They used a quasi-static approach to derive a so-called spring model (also presented by Tattersall [33]):

$$R = \frac{z_1 - z_2 + i\omega(z_1 z_2 / K)}{z_1 + z_2 + i\omega(z_1 z_2 / K)} \quad (1)$$

where z_1 and z_2 refer to is the acoustic impedance of the materials either side of the interface and ω is the angular frequency ($\omega = 2\pi f$). For identical materials in contact this reduces to ($z_1 = z_2 = z'$)

$$|R| = \frac{1}{\sqrt{1 + (K / \pi f z')}} \quad (2)$$

This model holds provided that the wavelength is large compared with the size of the gaps at the interface. The model demonstrates that the reflection coefficient also depends on the frequency used. Drinkwater *et al.* [16] carried out a series of experiments on rough surfaces pressed together. They observed the occurrence of frequency dependence of reflection and showed that when the simple spring model was used the stiffness was, as expected, frequency independent. They thus demonstrated that for most practically machined available rough surface contacts the spring model approach holds.

The stiffness of a rough surface contact K_a (expressed per unit area) is defined as the change in nominal contact pressure, p , required to cause unit approach of the mean lines of the surfaces [34]:

$$K_a = -\frac{dp}{dh} \quad (3)$$

where h is the separation of the mean lines of two rough surface (i.e. the mean interfacial separation). The stiffness of a rough surface contact varies non-linearly from zero at vanishingly small contact areas to infinity when the surfaces are a complete contact (i.e. further loading does not cause any a closer approach of the surfaces).

The stiffness of rough surface contacts under a range of loading configurations has been investigated by Dwyer-Joyce *et al.* [35]. The first loading takes place plastically and then unloading and subsequent re-loadings are largely elastic. The stiffness at a given pressure is thus lower during the loading path than during the unloading path.

(b) Lubricant film

An ultrasonic wave will also be reflected back from a thin oil film between two solid surfaces, shown by figure 1(d). Both the interfaces at the front and back of the oil film will act to reflect the wave. In most lubricated machinery the oil film is thin that these two reflections cannot be spatially separated. In this case when the wavelength is large compared to the thickness of the interface, it behaviours as a single reflector.

The same spring model approach as used for rough surface contacts can be applied to the measurement of lubricant films. A lubricant film acts as a compliant layer between the two mating surfaces. Rokhlin and Wang [36] addressed the ultrasonic interaction and spring stiffness for thin viscoelastic fluid films. Dwyer-Joyce *et al.* [35] showed that the oil films formed in conventional elastohydrodynamic and hydrodynamic regimes are also governed by the spring

model. It is the stiffness of the liquid layer that controls the ultrasonic reflection and the spring model equation (1) applies.

The oil film is considered as a fluid of bulk modulus, B between two infinite flat half spaces. The ultrasonic wave is again assumed to be larger compared with the gap thickness, h . This means that the film is constrained to deformation in the through thickness direction only. The stiffness of a liquid film is related to its thickness. Then the stiffness of the liquid layer is given by [37]:

$$K_l = \frac{B}{h} \quad (4)$$

(c) Mixed liquid-solid interface

In a mixed regime contact the interface consists of both liquid and solid bridges. At values of the film thickness greater than the surface roughness the interacting surfaces are fully separated by the lubricant and the fluid supports the total load (shown schematically in figure 1(d)), as the film thickness reduces the solid part becomes more significant (figure 1(c)).

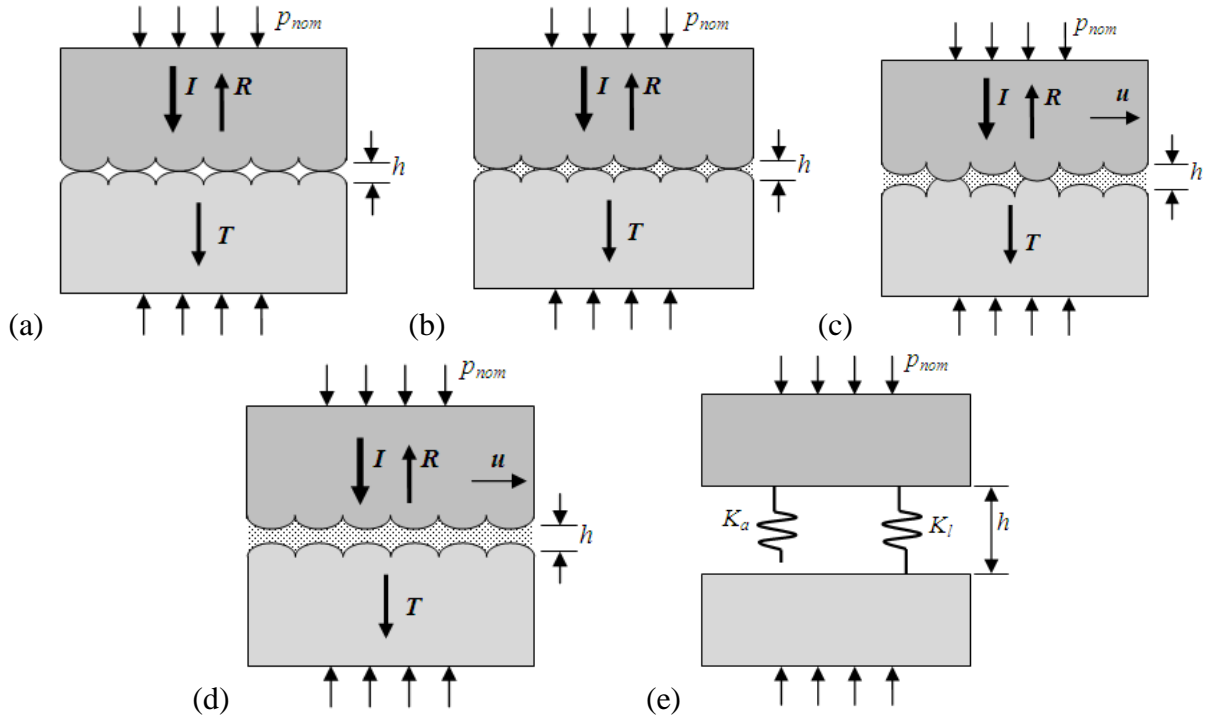


Figure 1 Schematic diagrams of tribological interfaces (a) a dry static contact, (b) a wet static contact, (c) mixed lubrication regime contact, (d) a thick oil film, (e) the spring model representation.

The total stiffness of the interface K_t , then results from the stiffness of the asperity contact, K_a and the stiffness of the liquid oil film, K_l acting in parallel (shown by figure 1(e)):

$$K_t = K_a + K_l \quad (5)$$

so combining equations (3),(4) and (5):

$$K_t = \frac{B}{h} - \frac{dp}{dh} \quad (6)$$

In this way the mixed regime interface is represented by two springs in parallel (figure 1(e)). At high surface separation, the asperity contact is negligible and, the dp/dh term falls to zero, the load is entirely carried by the liquid spring. For this reason the asperity spring in figure 1(e) is drawn not in contact with the lower surface. As the film thickness reduces, when a limiting value is reached, then solid contact is made and the spring has a finite stiffness. Conversely, at low separation both the stiffness of the thin liquid film and the asperity spring contribute to the solid stiffness.

In this work the reflection from an elastohydrodynamic circular point contact has been measured as the speed is reduced to zero. The reduction in speed causes the film thickness to fall; the contact moves from full film to mixed lubrication regime. The stiffness of the contact is determined and used to deduce the relative contributions of the asperity and film contributions.

3. Experimental apparatus

(a) Elastohydrodynamic point contact apparatus

The apparatus used was a modified optical elastohydrodynamic apparatus, where the microscope has been replaced by an ultrasonic transducer and the glass disk by a steel disk. Figure 2 shows both a photograph and a schematic diagram of the contacting parts. A 19 mm diameter steel ball was hydraulically loaded to the underside of a nominally flat steel disk. A pressure gauge recorded the hydraulic pressure and has been calibrated to obtain the ball contact force. Loads in the range 20 to 80 N were applied to the ball. According to an elastic calculation the corresponding areas of contact had radii of 0.11 to 0.174 mm and mean contact pressures in the range 0.53 to 0.84 GPa.

The ball is driven through a quill shaft by a variable speed electric motor and belt drive. The disk is held stationary throughout the testing so the contact is in pure sliding. Surface speed was set from zero to 0.5 m/s during this test. An ultrasonic transducer was located above the disk by a bath of distilled water and positioned over the contact using xyz positioning slides, shown in Figure 2(b).

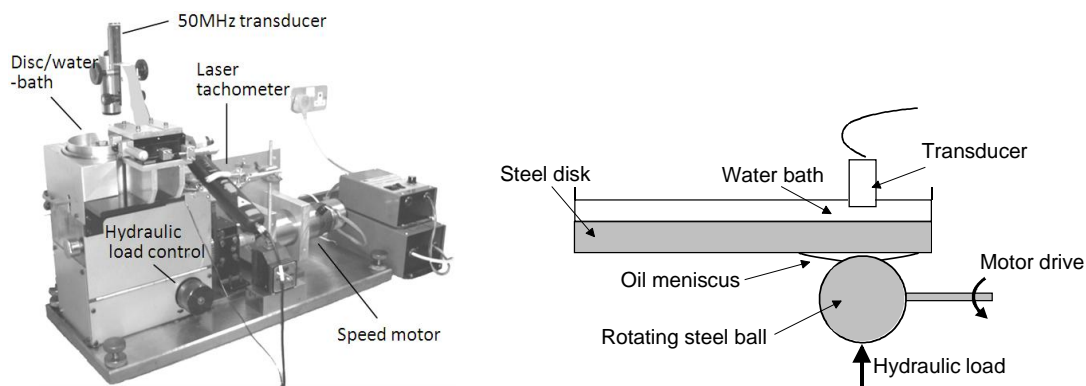


Figure 2 Elastohydrodynamic test apparatus for recording reflections from a lubricated ball on disk arrangement (a) photograph, (b) schematic diagram of the contact and transducer.

(b) Lubricants, specimens and test conditions

The test lubricant used was a VG68 mineral oil (Shell Turbo T68). The ball was half submerged in oil so that it was entrained into the contact when rotated. Both the ball (19mm in diameter) and disk were ground and lapped to give surface finishes of RMS roughness $\sigma = 0.256 \mu\text{m}$ and $\sigma = 0.339 \mu\text{m}$ respectively.

Corresponding author: Juanjuan ZHU, Paper No: TRIB-10-1223, page number 5

(c) Ultrasonic pulsing and receiving instrumentation

A spherical focusing longitudinal 50 MHz piezoelectric transducer (Olympus NDT) was used for this test case. The transducer was driven by an ultrasonic pulser receiver (UPR), which was controlled by a PC. The UPR generated a series of short duration voltage pulses that excited the piezoelectric transducer causing it to resonate, thus sending the required ultrasonic pulse through the medium. The transducer operated in pulse-echo mode and so received reflections back from the interfacial surfaces or oil film. Reflected pulses were stored on a digital oscilloscope and passed to a PC for processing. Figure 3 shows a schematic layout of the instrumentation.

The driver software was written in software program LabView which positioned the transducer, controlled the sequencing of pulses, downloaded reflected pulse waveforms, and performed the required signal processing. The reflection coefficient was recorded at each transducer position. This was then related to the interface stiffness and contact pressure. Full details of the experimental approach are given in reference [35].

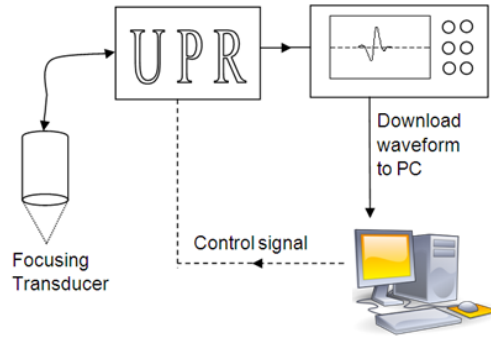


Figure 3 Schematic diagram of the ultrasonic pulsing and receiving apparatus.

4. Experimental results

(a) Transducer focussing and frequency selection

The transducer is focused onto the contact region. For the measurement to be realistic the whole of that focused region must fall within the confines of the lubricated contact. The dimensions of the focussed spot are given by [38]:

$$d_f = 1.025 \frac{Fc}{fD} \quad (7)$$

where d_f is the diameter of the spot size (where the signal has reduced to -6dB of its peak value), F is the transducer focusing length, f is the wave frequency, c is the wave speed in water and D is the diameter of the element. The radius of the contact region, a between the ball and disk is obtained from Hertz elastic analysis. The ratio of the spot size to the contact diameter is here called the focussing ratio, ϕ . Thus the frequency of the transducer should be selected such that this is less than one:

$$\phi = \frac{d_f}{2a} < 1 \quad (8)$$

Figure 4 shows a plot of the boundary of combinations of transducer frequency and load on the contact such that equation (8) holds. It is apparent for the measurement region (contact pressures

in the region 600 to 850 MPa) considered in this work that frequencies above around 20 MHz are required.

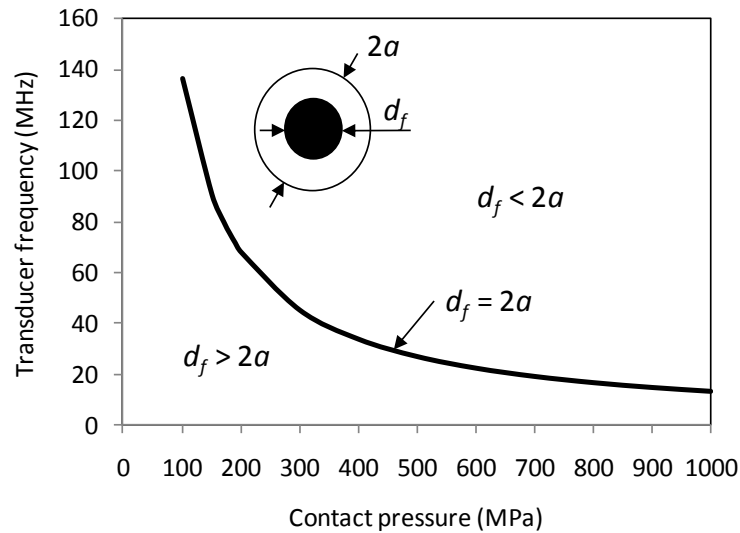


Figure 4. Relationship between the required transducer frequency and pressure on the contact such that the focussing ratio is smaller than one.

Figure 5 shows a plot of reflection coefficient amplitude versus frequency for a sample pulse reflected from an oil film under a pressure of 0.76 GPa (a load of 60 N) for ball and disc contact. Also shown is the amplitude spectrum fast Fourier transform (FFT) of the reflected pulse, showing the bandwidth region of useful energy. Inspection of the amplitude spectrum shows extent of the attenuation which has effectively reduced the centre frequency of the transducer from 50MHz to 30MHz. The reflection coefficient spectrum has been converted into the predicted oil film thickness using the spring model equation (1) and (4). The film thickness variation with frequency is also shown on figure 5. Clearly the oil film thickness cannot vary with the measurement frequency. Therefore only data in the 45 to 55 MHz region is suitable. Below 45 MHz the spot size is too large (as demonstrated in figure 5), and above 55 MHz the energy is too low as the transducer is operating out of its bandwidth. In this region the film is close to being constant regardless of the measurement frequency selected. This region of reflection coefficient can then be used to calculate layer stiffness.

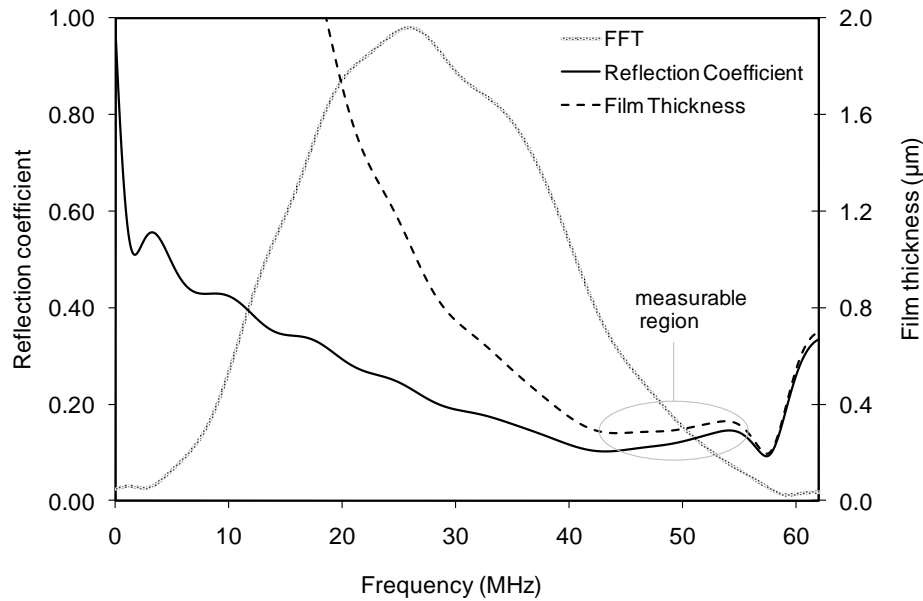


Figure 5 Reflection coefficient and oil film thickness plotted against ultrasonic frequency (the transducer output spectrum FFT is plotted in arbitrary units over the top). The measurable region were both the energy is acceptable and $\phi < 1$ is shown.

(b) The start up sequence

A simple start-up sequence was used to examine how the ultrasonic reflection varied during film formation. Figure 6(a) shows a plot of the reflection coefficient measured during the sequence; the sliding speed is plotted on the second y-axis. Initially the contact was completely dry and stationary. The ball was rotated by hand to cause the oil to be entrained into the contact, resulting in a stationary wet contact. The reflection was less than the dry contact case because there were lubricant pockets filling the valleys of the roughness in the contact. Transmission can then occur at the solid contact regions and through these lubricant pockets.

As the speed increased a film started to form and the reflection coefficient increased. The thicker oil film and less solid contact reflected more ultrasound. At some point during this speed ramp, lift off occurred, and the reflection was entirely caused by the liquid film.

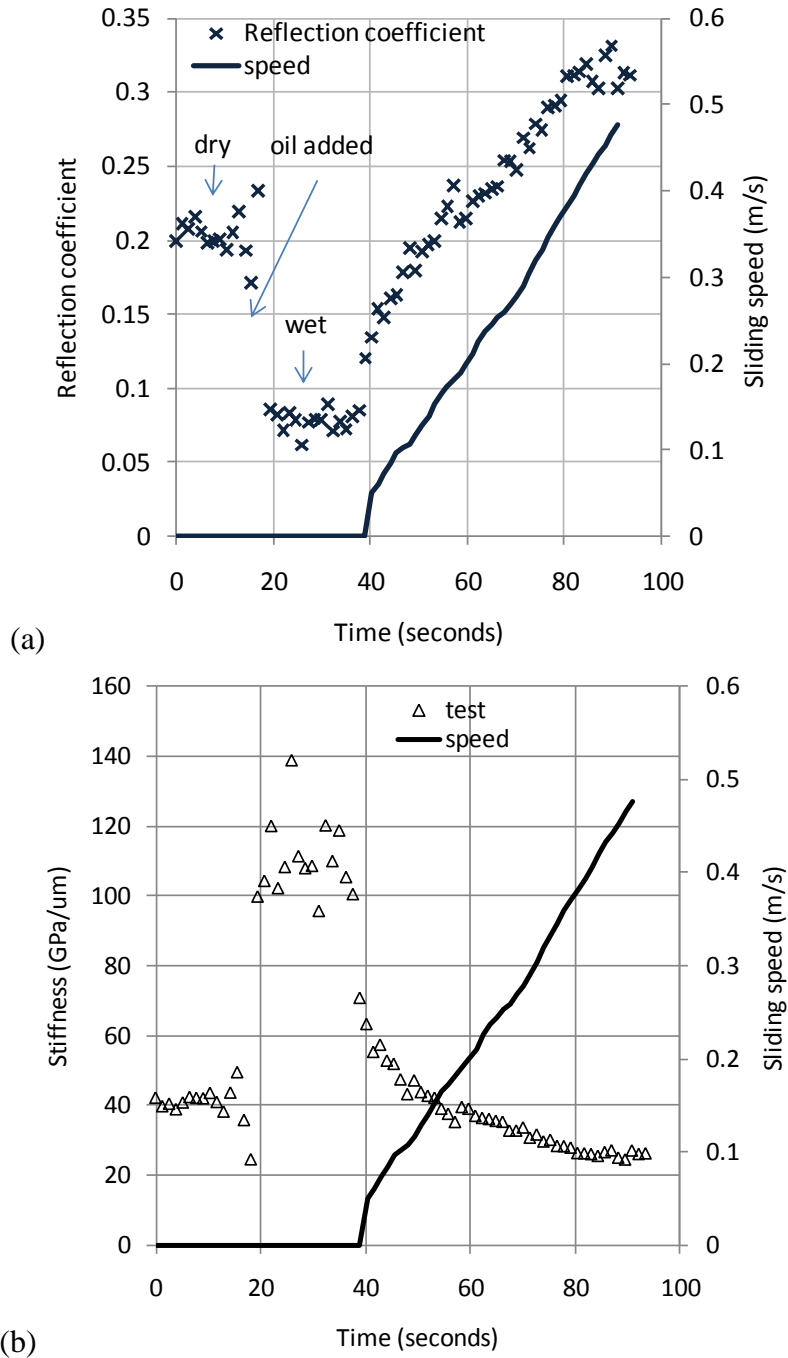


Figure 6 Measurements from a EHL contact mean contact pressure 0.76 GPa during a start-up (a) reflection coefficient (b) contact stiffness.

The spring model (equation 1) was used to convert reflection coefficient to stiffness; this is shown in figure 6(b). The stationary dry contact part had a stiffness of $K_a \sim 40$ GPa/ μm (there was no fluid present so $K_l = 0$). When the ball was stationary but fully wetted the contact stiffness increased by an additional ~ 70 GPa/ μm . This represents the contribution of the liquid part, K_l when stationary. In other words when the contact was stationary the total stiffness was 35%

attributable to the solid contacts and 65% to the liquid parts. As soon as sliding was initiated the stiffness decreased as the surfaces were separated by compressed liquid, some hydrodynamic action occurred.

(c) Smooth and rough surfaces

Figure 7 (a) and (b) compare two sets of results for disk specimens of different surface roughness ($\sigma=0.34$ and $0.03\mu\text{m}$). For the smooth surface case the surfaces were polished by hand to a mirror finish. The data shows the stiffness variation with load for when the contact is dry, fully wetted, and sliding at 0.15m/s .

For the dry case the smooth surface is stiffer for a given load. For the wet case this is again true; but in this case since the smooth surface holds only a very thin layer, of consequently high stiffness, between the surfaces. When both pairs are sliding, they have virtually identical stiffness. This is because a hydrodynamic film has formed and the stiffness is only from the fluid film. The surface roughness clearly has no part in the film development at this sliding speed.

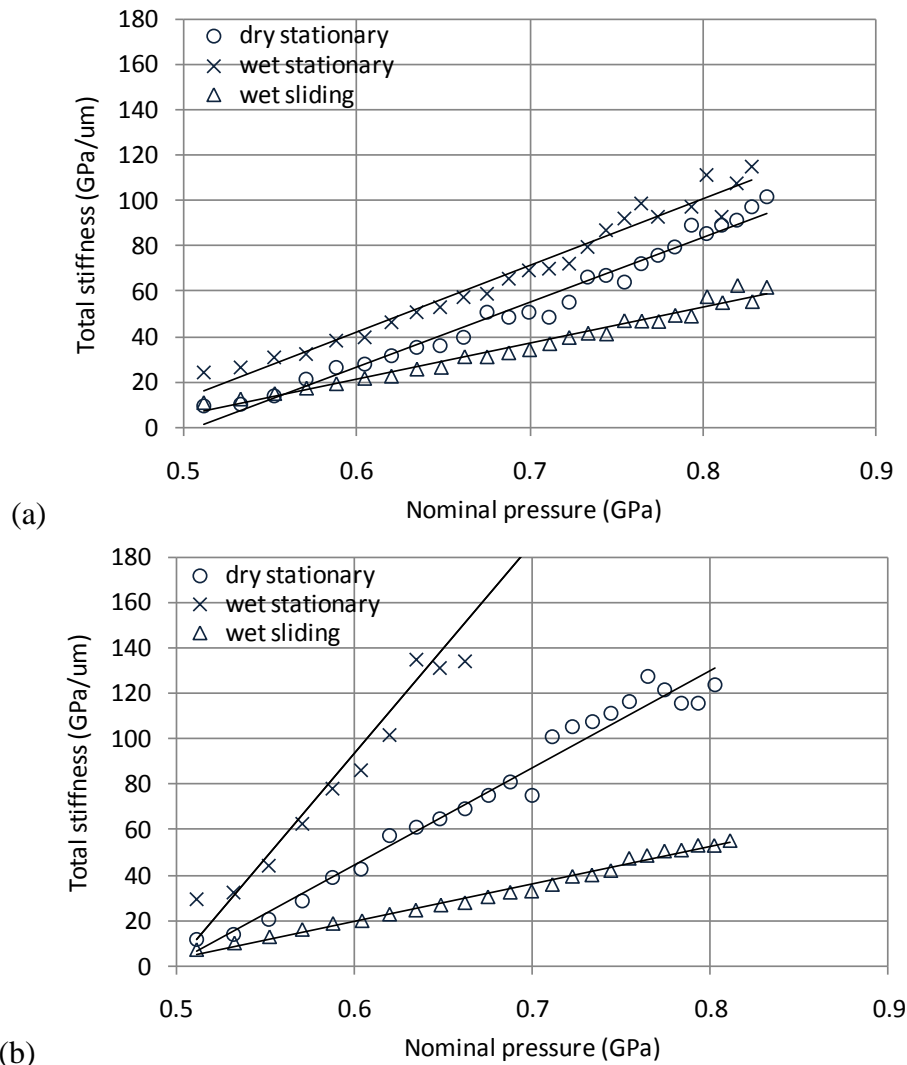


Figure 7 Variation of stiffness with contact load for different surfaces roughness (a) standard surface roughness ($\sigma=0.34 \mu\text{m}$), (b) mirror finish polished surfaces ($\sigma=0.03 \mu\text{m}$).

5. Theoretical simulation

The proceeding results show qualitatively how the ultrasonic reflection can be used to determine the sum of the asperity contact stiffness and the liquid film stiffness. Just as when a mass is supported by two springs, it is not possible to determine the proportion supported by each spring from the combined stiffness. Some independent means is required to determine the relative proportion of liquid and solid contact from the total stiffness. However, unlike the analogy of a mass supported by two springs, in the mixed lubrication case the two spring stiffness are not independent. Both springs are of non-linear stiffness that depends on the separation of the two surfaces. In this section, models for the spring stiffness are derived and used in section 6 to interpret the ultrasonic results.

(a) Stiffness of static dry contact

The contact between rough surfaces has been investigated by many authors. Three typical models of rough surface contact are (i): the Greenwood-Williamson model [39]; (ii): the Whitehouse-Archard-Onions model [40, 41]; (iii): the Bush-Gibson-Thomas model [42], which are referred as GW, WAO and BGT model respectively. The GW and BGT models are based on purely elastic deformation. In this work on rolling circular point contacts, high pressures are expected and also repeated contact of different asperity pairs. This suggests that elastic-plastic or plastic deformation may take place at the peaks of the ball and disc roughness. For this reason, the WAO model is adopted for the dry contact case. In this model the distribution of the asperity summits is not Gaussian but results from the Gaussian distribution of the surface as a whole. The radiuses of the asperities are not constant: the higher summits give smaller radius and vice versa. The WAO model gives a relationship between the nominal contact pressure and the approach of the two surface mean lines.

$$p = \frac{4}{15} (5D_s)^{1/2} E' \sigma_s F_p(t) \quad (9)$$

Where σ_s is the variance of the summit height distribution, and D_s is their density expressed per unit area. The ratio t is the dimensionless separation of contacting surfaces ($h = t\sigma_s$), and E' is the reduced elastic modulus given by:

$$\frac{1}{E'} = \frac{1-\nu_b^2}{E_b} + \frac{1-\nu_d^2}{E_d} \quad (10)$$

where E and ν are the elastic modulus and Poissons ratio, with the subscripts b and d signifying the ball and disc respectively.

$F_p(t)$ is a dimensionless separation function which is tabulated in Whitehouse and Archard [41] with a quite good approximation in analytical form as:

$$F_p(t) = 0.612 \exp(-0.4t^2 - 1.3t) \quad (11)$$

Królikowski and Szczepek [14] use the WAO model to predict the interface stiffness. They give an analytical curve fit to the data;

$$K_a = -\frac{dp}{dh} = \frac{p}{\sigma_s} \left[1.7 - 1.6 \log_e \left(\frac{2.7p}{E'D_s^{1/2}\sigma_s} \right) \right]^{1/2} \quad (12)$$

Equation (12) is used in this work to predict stiffness for the static dry contact.

(b) Stiffness of static wet contact

If the interface is submerged in oil, surface tension, or a small relative movement between the contacting surfaces, will draw in liquid to fill the pockets between the asperity contacts. If the load is increased the two interfaces approach and extrude a finite but very small volume of lubricant (figure 1(b)). When ultrasonic waves strike this interface some will pass through the asperity contact and others the lubricant pockets. Therefore, for a wet interface the total interfacial stiffness has two components: the solid stiffness arising from the mechanical asperity interaction, and the lubricant stiffness attributable to the lubricant pockets.

The surface roughness has a random distribution, and the real area of contact is relatively small compared to the apparent area. It is therefore reasonable to assume that the lubricant can freely flow between the valleys (i.e. there are no trapped and isolated pockets of lubricant). This means that the oil is under ambient atmospheric pressure, even though asperities contacts are under a very much greater pressure. The stiffness of the asperities contacts can be obtained from equation (12). The separation of the mean lines of the surface roughness is obtained from equation (9). This is then used in equation (4) to get the liquid stiffness.

The total stiffness is then

$$K_t = K_a + K_l = \frac{P}{\sigma_s} \left[1.7 - 1.6 \log_e \left(\frac{2.7P}{E'D_s^{1/2}\sigma_s} \right) \right]^{1/2} + \frac{B_0}{h}$$

Where the bulk modulus for the oil at ambient pressure, B_0 is used, equation (15) is used to calculate B_0 as 1.339 GPa (see also table 1).

(c) Stiffness of a liquid film

The stiffness of an oil film, equation (4), depends on its thickness and the bulk modulus. The latter can be easily determined from its acoustic properties according to:

$$c = \sqrt{\frac{B}{\rho}} \quad (13)$$

Where c is the speed of sound through the liquid and ρ is its density. The speed of sound in a sample of oil can readily be measured (using a time of flight method) and the bulk modulus deduced. This is quite satisfactory for application in low pressure hydrodynamic cases [26]. However in elastohydrodynamic lubrication the oil is subject to high pressure and so its bulk modulus changes significantly.

Measuring the bulk modulus under such conditions is difficult. Normally this would require a high pressure chamber [43, 44]. Kondo et al. [45] have used an ultrasonic approach on an EHL contact where an optical interference method was used to determine the film thickness independently. This was then used in equation (4) to determine the bulk modulus.

In this study, the analysis of [46] is used to calculate the bulk modulus of the compressed lubricant, according to:

$$B = \left\{ 1 - \frac{1}{1+B_0'} \log_e \left[1 + \frac{p}{B_0} (1+B_0') \right] \right\} \left[B_0 + p (1+B_0') \right] \quad (14)$$

Where p is the pressure in liquid; B_0 is the bulk modulus at ambient pressure ($p=0$); B_0' is the pressure rate of change of B at ambient pressure, which is approximately 11. B_0 is described by Fakhreddine and Zoller [47], as

$$B_0 = B_{00} \exp(-\beta_k T) \quad (15)$$

Where B_{00} is approximately 9 GPa and β_k is approximately $6.5 \times 10^{-3} K^{-1}$, T is the absolute temperature.

Bair [46] stated that this equation is often considered to be the most accurate [48] and even accurate for extrapolation to very high pressures [49]. It has been used successfully by Cook *et al.* [50] in a free volume pressure-viscosity correlation. The mean values of pressure are used in equation (14) for lubricant bulk modulus. The ultrasonic vibration is very low amplitude and high speed. It is therefore an isentropic process and so it is the adiabatic bulk modulus that is the relevant fluid property. Table 1 shows the bulk modulus values calculated for use in this work.

Load, N	Pressure, GPa	Bulk modulus, GPa
0	0	1.339
10	0.420	5.546
20	0.529	6.565
30	0.605	7.269
40	0.666	7.823
50	0.718	8.287
60	0.763	8.691
70	0.803	9.049
80	0.839	9.374

Table 1 Lubricant bulk modulus values (determined after the analysis of Bair [46]) at the test pressures used in this work.

The stiffness of the fluid film is then the bulk modulus, at the appropriate test contact pressure, defined by equation (14) divided by the oil film thickness.

(d) Stiffness of mixed lubrication contact

In the case of a sliding contact, oil is entrained between the surfaces and a hydrodynamic pressure is generated. If the sliding speed is sufficiently high then a full film occurs and there is no asperity contact. Equation (4) can then be used to determine the stiffness of the contact which is now entirely supported by liquid.

If however the lubricant film thickness is less than the surface roughness then both the hydrodynamic film and the asperity contacts contribute to the total stiffness according to equation (6). In this section an equation set is built to predict the load sharing proportions and surface

separation, and from these K_a and K_l . The method follows the approach of [6, 51] where the film formation is modelled independently of asperity contact.

The total load supported on the contact, P_T is the sum of the loads supported by the asperities, P_a and the liquid bridges, P_l :

$$P_T = P_a + P_l$$

This equation can be written in terms of two scaling factors (after the method of [5]), γ_1 and γ_2 , where

$$\begin{aligned}\gamma_1 P_l &= P_T \\ \gamma_2 P_a &= P_T\end{aligned}\quad (16)$$

Then:

$$\frac{1}{\gamma_1} + \frac{1}{\gamma_2} = 1 \quad (17)$$

For the rough surface contact part of the analysis the Greenwood and Williamson [39] model is used. The load supported by asperities is:

$$P_a = p_a A_0 \quad (18)$$

Where p_a is the nominal contact pressure and A_0 is the nominal contact area. Greenwood and Williamson give the contact pressure in a rough surface interface as,

$$p_a = \frac{4}{3} D_s E' R_s^{1/2} \sigma_s^{3/2} F_{3/2}(t) \quad (19)$$

Where R_s is the mean radius of the summits, $F_{3/2}(t)$ is an integral of summit height distribution, Usually this distribution of asperity heights as assumed to be Gaussian distribution, and in that case the function F_n becomes:

$$F_n(t) = \frac{1}{\sqrt{2\pi}} \int_t^\infty (s-t)^n e^{-s^2/2} ds \quad (20)$$

According to Hertzian contact theory the nominal contact area for circular point contact is

$$A_0 = \pi \left(\frac{3PR'}{4E'} \right)^{2/3} \quad (21)$$

Where P is the applied load, R' is the reduced radius of two contact bodies (in the present case of a ball sliding on a flat disc, R' is equal the radius of the ball).

Combining equations (19) and (21), the load becomes,

$$P_a = \frac{4}{3} \pi D_s E' R_s^{1/2} \sigma_s^{3/2} \left(\frac{3PR'}{4E'} \right)^{2/3} F_{3/2}(t) \quad (22)$$

This is the load supported by the asperities in the mixed regime contact or P_T / γ_2 .

Replacing E' by E'/γ_2 and D_s by D_s/γ_2 (after [6]) gives:

$$\frac{P_T}{\gamma_2} = \frac{4}{3} \pi D_s E' R_s^{1/2} \sigma_s^{3/2} \left(\frac{3P_T R'}{4E'} \right)^{2/3} F_{3/2}(t) \quad (23)$$

We now turn to the determination of the lubricant film thickness. The film thickness equation for point contact has been developed by Hamrock and Dowson [52, 53] for the full film case:

$$H = 2.69U^{0.67} G^{0.53} W^{-0.067} (1 - 0.61e^{-0.73}) \quad (24)$$

Where H , W , U , and G are a set of dimensionless parameters are defined as follows:

$$H = \frac{h}{R'}, \quad W = \frac{P_l}{2E'R'^2}, \quad U = \frac{\eta_0 u}{2E'R'}, \quad G = 2\alpha E'.$$

where η_0 is the inlet viscosity at ambient pressure, u is sliding speed, and α is the pressure-viscosity index, which can be obtained by plotting the natural logarithm of dynamic viscosity versus pressure. The slope of the graph is the pressure-viscosity index.

Again the scaling factors are used to apportion the load supported by the hydrodynamic film. Substituting E'/γ_1 for E' and P_T/γ_1 for P , the film thickness equation for mixed lubrication can be rewritten as,

$$\frac{h}{R'} = 1.899 \left(\frac{\eta_0 u \gamma_1}{2E'R'} \right)^{0.67} \left(\frac{2\alpha E'}{\gamma_1} \right)^{0.53} \left(\frac{P_T}{2E'R'^2} \right)^{-0.067} \quad (25)$$

Equations (17), (23), and (25) form a set of simultaneous equations with three unknown variables, γ_1 , γ_2 and h . These three parameters are then used to calculate lubricant stiffness and asperity contact stiffness from equations (4) and (12) separately. Then equation (6) is used for calculation of total interfacial contact stiffness.

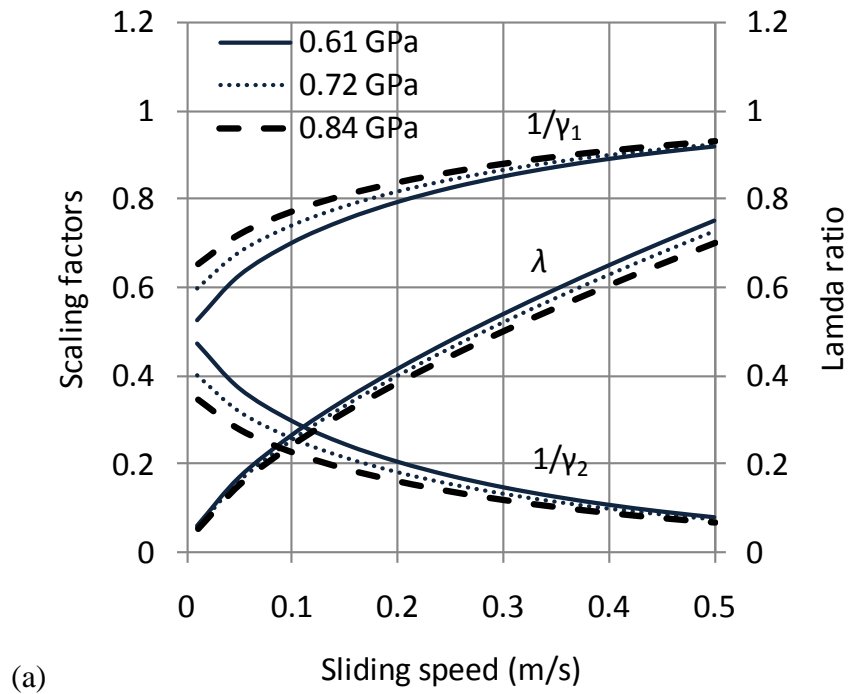
The simultaneous equations were solved using MathCAD. Table 1 gives the parameters used in the model. The asperity parameters were obtained from profiles of the ball and disk surfaces recorded using a Mitutoyo stylus profilometer. Lubricant and materials property data are datasheet values.

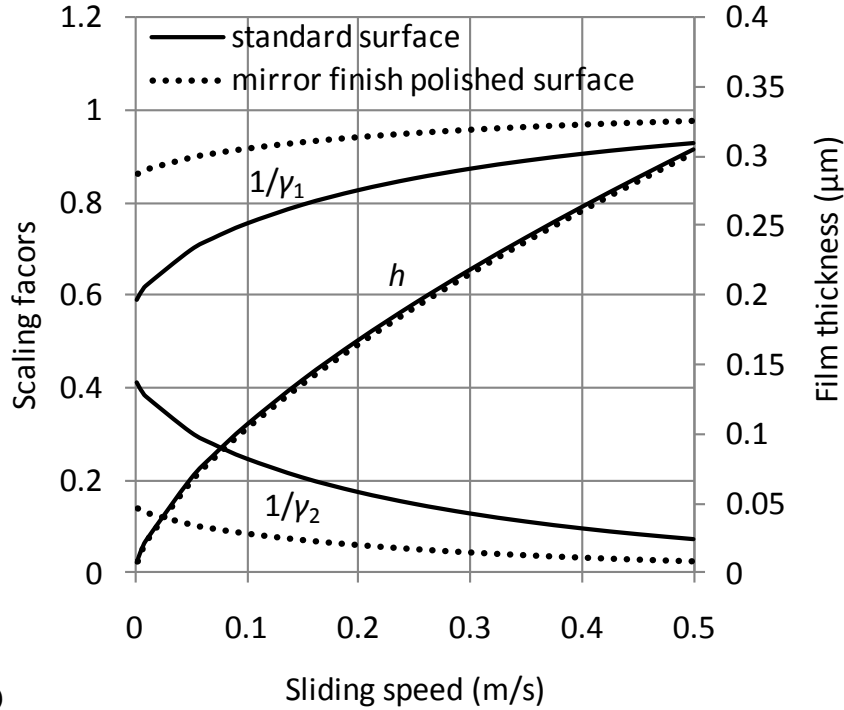
Parameter	Symbol	Value
Elastic modulus of steel ball and disc	E	200 GPa
Poisson's ratio of steel ball and disc	ν	0.31
Radius of ball	R'	19 mm
Asperity density	D_s	$1.97 \times 10^{10} \text{ m}^{-2}$
Mean radius of asperity summits	R_s	2.7 μm
Standard deviation of asperity summit heights	σ_s	0.3 μm
Lubricant viscosity at inlet temperature	η_0	0.095 Pa·s
Pressure-viscosity index	α	25.1 GPa^{-1}

Table 2 Parameters used in the simulation model

(e) Simulation results

Figures 8 (a) and (b) show the output from the mixed lubrication model; the proportions of load supported by liquid and solid contact are shown varying as the speed is increased. Also shown is the film thickness and lambda ratio, λ (ratio of the oil film thickness to the combined rms surface roughness $\lambda = h/\sqrt{\sigma_1^2 + \sigma_2^2}$).





(b) Figure 8 Simulation result for the mixed lubrication regime scaling factors and Lambda ratio/film thickness for (a) three nominal contact pressures (b) two different surface finishes under a pressure of 0.76 GPa.

The proportions of hydrodynamic lifting force (expressed as $1/\gamma_1$) and the lubricant film thickness clearly increase with velocity, indicating almost full separation at a speed of 0.5 m/s. At low speed there is appreciable solid contact indicated

Figure 8 (b) shows the comparison of the prediction for the standard rough surface compared with the mirror finish polished surface both under a pressure of 0.76 GPa. In this figure the scaling factors show significant difference but the film thicknesses are almost the same for two surfaces. For smooth surface case, asperity interaction contributes little in sharing applied load.

Figure 9 demonstrates how the stiffness varies according to this model. It is immediately evident that the liquid component of stiffness is very much higher than the solid part. Essentially this is because whilst the modulus of a liquid is lower, the layer thickness is very much thinner, and so it is inherently stiffer.

The effect of pressure on the total and asperity stiffness is shown in Figure 9(a). The locations of lambda ratio 0.5, 1 and 1.5 are also plotted in this figure to show the increasing contribution of lubricant to the load sharing. In all cases as the sliding speed reaches 1.5m/s, lambda is greater than around 1.5 the asperity stiffness falls close to zero.

Comparison between the compressed lubricant stiffness K_l and asperity contact stiffness K_a are shown in Figures 9 (b), (c) and (d). The ratio of K_l/K_a changing with sliding speed and nominal pressure are simulated and shown in Figure 9 (c) and (d) individually. The inversion in Figure 9 (c) is caused by the faster rate of reduction in stiffness as the film tends to zero. Liquid stiffness is inversely proportional to thickness and therefore K_l tends rapidly to infinity. The reduction in

solid stiffness as the surfaces approach is more gentle. It is clear that in all cases compressed liquid plays the main part in supporting the applied load.

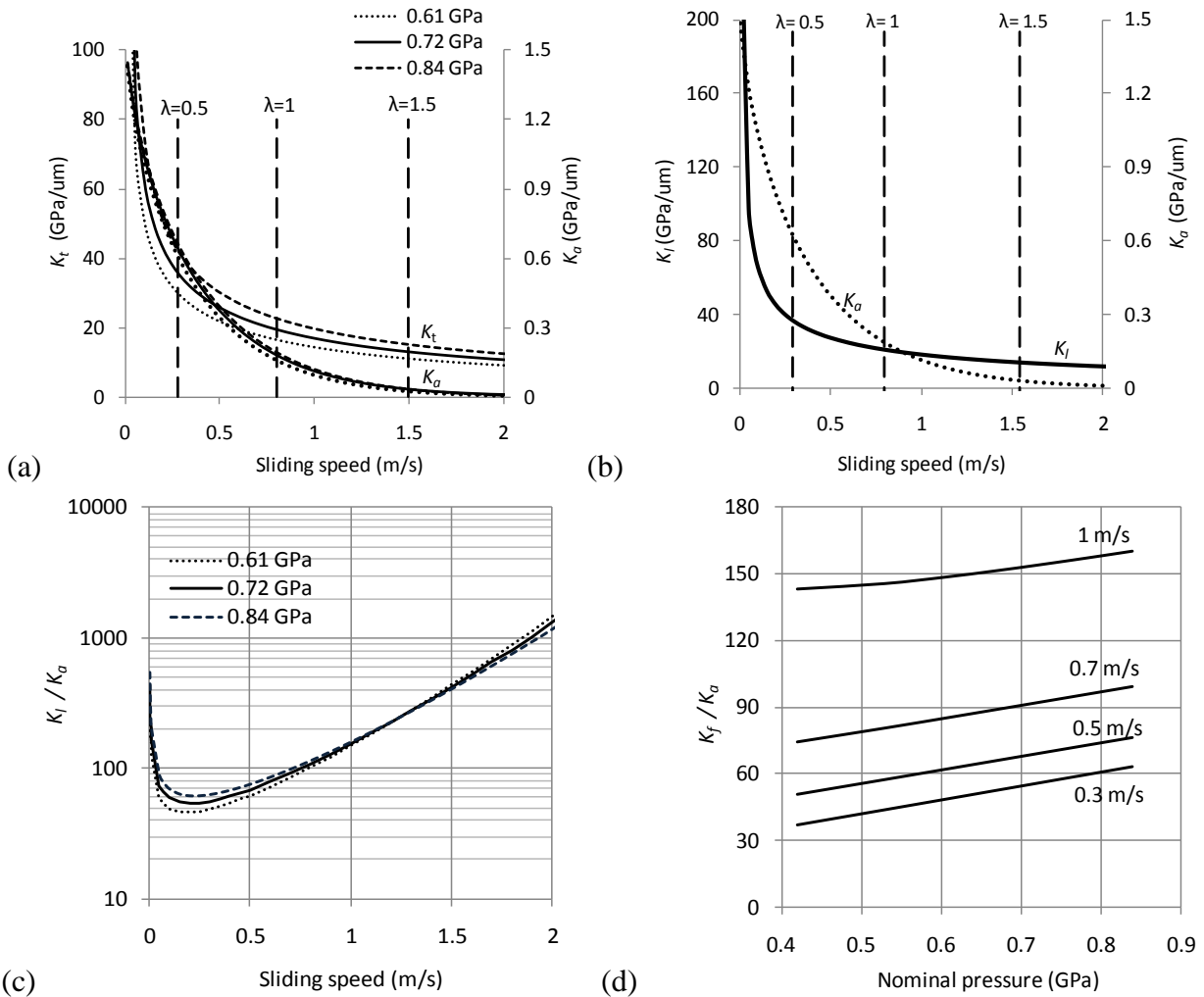


Figure 9 Comparison of stiffness, K_l , K_a and K_t (a) total and asperity stiffness variation with load and speed, (b) liquid and asperity stiffness variation with speed, (c) ratio of liquid to asperity stiffness variation with speed, (d) ratio of liquid to asperity stiffness variation with load.

6. Comparison and discussion

Figure 10 shows the predicted stiffness from the mixed lubrication model compared with experimental data for six load cases. Simulations of dynamic stiffness for different loads show a good agreement with experimental measurements. As the sliding speed increases the separation increases the proportion of load shared by asperity contacts gives a reducing asperity stiffness based on equation (12). At the higher speeds the total interfacial stiffness here is mostly contributed by compressed liquid.

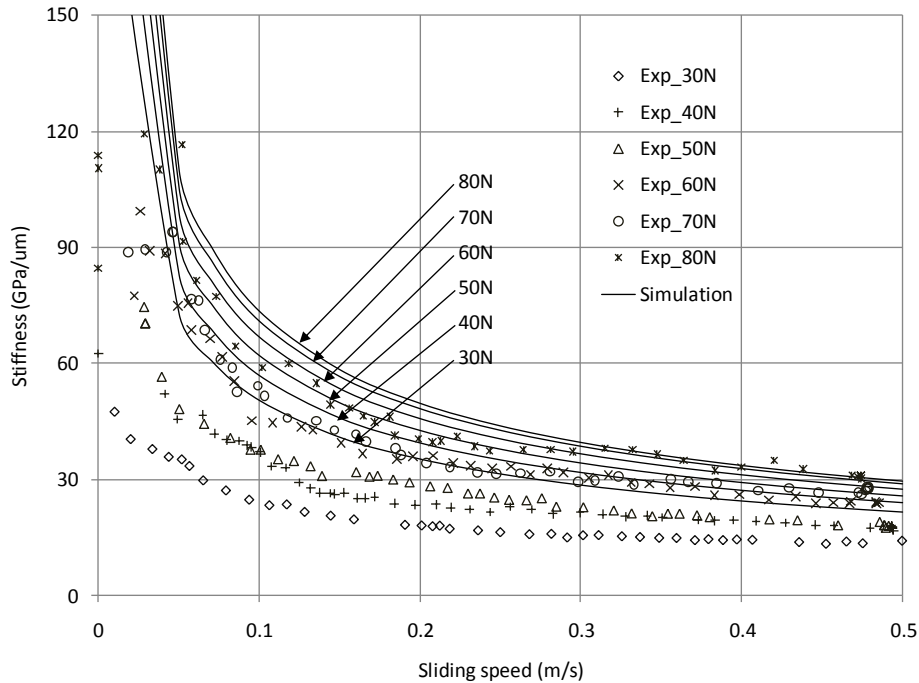


Figure 10 Comparison of measured stiffness and simulation stiffness varying with sliding speed for a series of different contact loads

The mixed lubrication model was used to determine the ratio of liquid stiffness to asperity stiffness at each speed data point for the contact pressures of 0.61, 0.72 and 0.84 GPa (loads 30, 50, 80 N). This ratio was then used with the experimental data to separate stiffness contributions from compressed oil and asperity contact. Figure 11 shows the results.

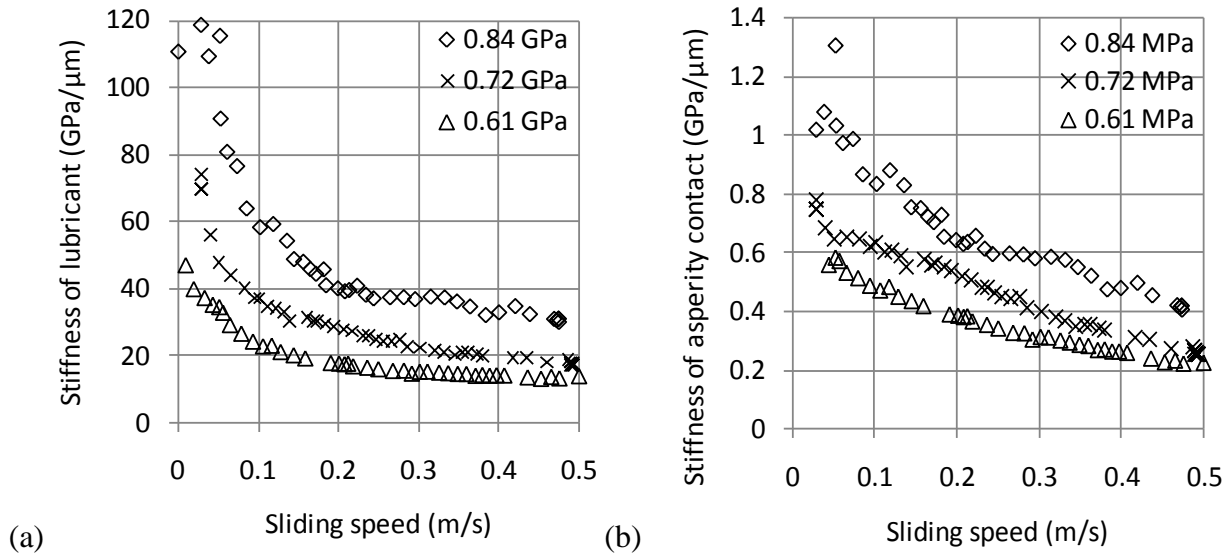


Figure 11 Experimental stiffness of mixed regime contact. The mixed lubrication model has been used to determine the stiffness ratio and to separate the (a) stiffness of lubricant film, and (b) the stiffness of asperity contact, from the measured combined stiffness (data of Figure 10).

Once the stiffness components have been separated out, the oil film thickness is easily determined using equation (4). This is plotted on figure 12 for each of the three load cases. The non-dimensional speed and load axes corresponding to the Hamrock and Dowson equation (24) are used so that the data should all collapse onto one curve if that model holds.

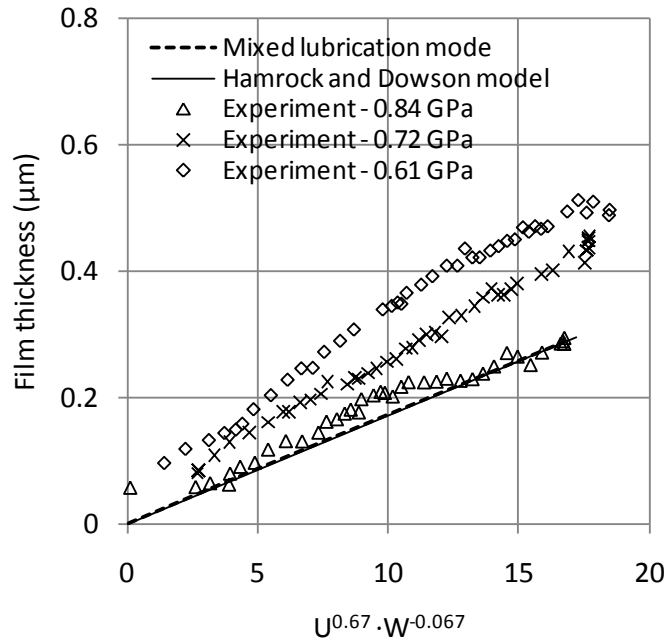


Figure 12 Comparison of film thickness against dimensionless parameter at $p=0.84\text{GPa}$

Also plotted on figure 12 is the oil film thickness prediction using the mixed regime model, and that using the standard full film Hamrock and Dowson model (equation 24). The difference between the two models is very small. The higher load experimental data closely fits the model. At the two lower loads, whilst the slope is similar, the agreement is not so good.

Figure 13 shows the mixed regime model, and the static dry and wet stiffness models compared with experiment during a start-up cycle. The prediction of the full film Hamrock and Dowson case is also shown (the stiffness becomes infinite when the speed and film thickness tend to zero). As expected the dynamic lubrication part agrees well. It is apparent that in the region of the graph $40 < t < 100$ sec a continuous film was formed; and the fluid film stiffness shows close agreement with the mixed lubrication prediction. At around 40 sec as the speed tends to zero the predicted oil film stiffness rises to infinity as $h \rightarrow 0$. The measured value tends to a finite stiffness of ~ 120 GPa as the contact consists of rough asperity interactions and not a thin layer.

The simulation gives the dry contact stiffness at $5.6 \text{ GPa}/\mu\text{m}$, which is some eight times lower than the measured value. A similar large discrepancy is observed in the wet static contact. The agreement between models of dry asperity contact and ultrasonic data is difficult to achieve. Poor agreement has also been observed in earlier work in this area [14, 16].

Perhaps the source of error is the difficulty in measuring surface roughness. Roughness parameters are dependent on the measurement scale used [54] and it is likely that the measurement scale imposed by a stylus profilometer differs significantly from that of an ultrasonic wave striking the asperity. This is an issue that remains to be resolved. Closer

agreement with experimental data for these dry contact is observed using the modelling approach where roughness data is obtained by fitting ultrasonic data to model predictions [18, 23].

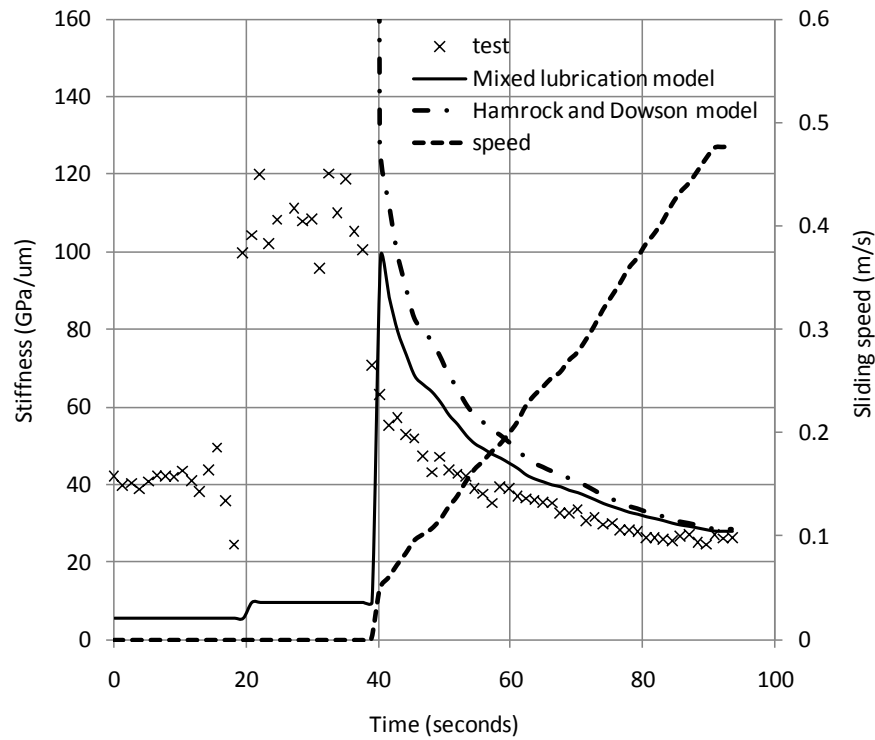


Figure 13 interface contacting stiffness with the pressure of 0.76GPa

7. Conclusions

A method based on the reflection of ultrasonic waves has been used to measure the contact stiffness of a lubricated steel ball sliding on a steel disc as the regime changes from static, through mixed, to full film. The resultant stiffness measurement is the sum of liquid and asperity contact stiffness combined in parallel. Stiffness values in the range 10 to 120 GPa/ μm were recorded for a range of contact loads and sliding speeds.

A model of the mixed lubrication process was built using a set of three simultaneous equations, representing; load sharing, asperity contact, and elastohydrodynamic film thickness. This model was used to predict the liquid and asperity stiffness components. For all operating cases the liquid stiffness is very much higher than the solid stiffness. This is because whilst the liquid has an intrinsically lower modulus than the solid (even at the elevated contact pressures it experiences) the layer is very thin and so therefore very stiff. The total interfacial stiffness simulated shows reasonable agreement with experimental results.

The ultrasonic measurements yield only a combined liquid and asperity stiffness. Here we have used the mixed regime model to determine the expected ratio of these two parameters at each load and speed data point. This ratio has then been used to separate the two stiffness components, and hence determine the oil film thickness. This demonstrates one approach in which a model can be used to extract useful information from the ultrasonically measured data.

Predictions of the overall mixed regime behaviour agree well with experimental data. However, in this regime it is the lubricant stiffness that dominates. The prediction of this parameter, by combining the model of Hamrock and Dowson [52,53] with the lubricant rheology model of Bair [46] gives good results. However, when only the static asperity contact part is modelled, using the statistical asperity contact models, agreement with experimental data for dry contact is much less convincing.

Nomenclature

a	half width of Hertzian contact
A_0	Nominal contact area
B	Bulk modulus
B_0	Bulk modulus at atmospheric pressure
c	speed of sound through the liquid (i.e. oil)
d_f	diameter of the transducer spot size
D	diameter of the transducer element
D_s	asperity density
E	elastic modulus
E'	reduced elastic modulus
F	transducer focal length
f	ultrasonic wave frequency
h	oil film thickness, separation of the mean lines of two rough surfaces
K	stiffness
p	contact pressure
P	applied load
R	ultrasonic reflection coefficient
R'	radius of ball
R_s	mean radius of asperity summits
t	dimensionless separation of contacting surfaces
T	absolute temperature
u	sliding velocity
z	acoustic impedance of the material
α	pressure-viscosity index
γ	scaling factor
η_0	Lubricant viscosity at inlet temperature
λ	film thickness parameter
ν	Poissons ratio
ρ	density of liquid (i.e. oil)

Corresponding author: Juanjuan ZHU, Paper No: TRIB-10-1223, page number 22

- σ Root mean square roughness
- σ_s standard deviation of asperity summit heights
- ϕ ratio of the spot size to the contact diameter
- ω ultrasonic angular frequency ($\omega = 2\pi f$)

References

- [1] Spikes, H. A., 1999, "Thin films in elastohydrodynamic lubrication: the contribution of experiment," Proc. Inst. Mech. Eng. Part J: J. Eng. Tribol., 213, pp. 335-352.
- [2] Tsao, Y. H., and Tong, K. N., 1975, "A Model for Mixed Lubrication," ASLE Transactions, 18(2), pp. 90-96.
- [3] Soda, N., 1985, "Effect of Abbott Bearing Area on Characteristics of Stribeck Curve," Journal of Japanese Society of Tribologists, 31, pp. 637-642.
- [4] Yamaguchi, A., and Matsuoka, H., 1992, "A Mixed Lubrication Model Applicable to Bearing/Seal Parts of Hydraulic Equipment," ASME J. Tribol., 114, pp. 116-121.
- [5] Johnson, K. L., Greenwood, J. A., and Poon, S. Y., 1972, "A Simple Theory of Asperity Contact In Elastohydrodynamic Lubrication," Wear, 19, pp. 91-108.
- [6] Gelinck, E. R. M., and Schipper, D. J., 2000, "Calculation of Stribeck Curves for Line Contacts," Tribol. Int., 33, pp. 175-181.
- [7] Tallian, T.E., Chiu, Y.P., Huttenlocher, J.A., Kamenshine, J.A., Sibley, L.B., and Sindlinger, N.E., 1964, "Lubricant Films in Rolling Contact of Rough Surfaces," ASLE Transactions, 7, pp. 109-126.
- [8] Johnson, G. J., Wayte, R., and Spikes, H. A., 1991, "The Measurement and Study of Very Thin Lubricant Films in Concentrated Contacts," Tribology Transactions, 34, pp. 187-194.
- [9] Spikes, H. A., and Olver, A.V., 2003, "Basics of Mixed Lubrication," Lubrication science, 16, pp. 4-28.
- [10] Guangteng, G., Cann, P. M., Olver, A. V., and Spikes, H. A., 2000, "An Experimental Study of Film Thickness Between Rough Surfaces in EHD Contacts," Tribol. Int., 33, pp. 183-189.
- [11] Kendall, K., and Tabor, D., 1971, "An Ultrasonic Study of the Area of Contact Between Stationary and Sliding Surfaces," Proc. R. Soc. A, 323, pp. 321-340.
- [12] Arakawa, T., 1983, "A Study on the Transmission and Reflection of an Ultrasonic Beam at Machined Surfaces Pressed against Each Other," Materials Evaluation, 41, pp. 714-719.
- [13] Królikowski, J., Szczepek, J., and Witczak, Z., 1989, "Ultrasonic Investigation of Contact Between Solids under High Hydrostatic Pressure," Ultrasonics, 27, pp. 45-49.
- [14] Królikowski, J., and Szczepek, J., 1991, "Prediction of contact parameters using ultrasonic method," Wear, 148, pp. 181-195.
- [15] Minakuchi, Y., Yoshimine, K., Koizumi, T., and Hagiwara, T., 1985, "Contact Pressure Measurement by Means of Ultrasonic Waves (on a method of quantitative measurement)," Bull. JSME, 28 (235), pp. 40-45.
- [16] Drinkwater, B. W., Dwyer-Joyce, R. S., and Cawley, P., 1996, "A Study of the Interaction Between Ultrasound and a Partially Contacting Solid-Solid Interface," Proc. R. Soc. A, 452, pp.2613-2628.
- [17] Nagy, P.B., 1992, "Ultrasonic classification of imperfect interfaces," Journal of Non-destructive Evaluation, 11, Nos. 3/4, pp.127-139.
- [18] Baltazar, A., Rokhlin, S.I., and Pecorari, C., 2002, "On the Relationship between Ultrasonic and Micromechanical Properties of Contacting Rough Surfaces," Journal of the Mechanics and Physics of Solids, 50, pp. 1397-1416.
- [19] Dwyer-Joyce, R. S., Drinkwater, B. W., and Quinn, A.M., 2001, "The Use of Ultrasound in the Investigation of Rough Surface Interfaces," ASME J. Tribol., 123, pp. 8-16.
- [20] Kim, J.-Y., Baltazar, A., Rokhlin, S.I., 2004, "Ultrasonic assessment of rough surface contact between solids from elastoplastic loading-unloading hysteresis cycle," Journal of the Mechanics and Physics of Solids, 52, pp. 1911 -1934.

Corresponding author: Juanjuan ZHU, Paper No: TRIB-10-1223, page number 23

- [21] Kim, J.-Y., Baltazar, A., Hu, J.W., Rokhlin, S.I., 2006, "Hysteretic linear and nonlinear acoustic responses from pressed interfaces," *International Journal of Solids and Structures*, 43, pp. 6436-6452.
- [22] Biwa, S., Hiraiwa, S., Matsumoto, E., 2007, "Stiffness evaluation of contacting surfaces by bulk and interface waves," *Ultrasonics*, 47, pp. 123-129.
- [23] Pecorari, C., and Poznic, M., 2006, "On the linear and nonlinear acoustic properties of dry and water-confining elasto-plastic interfaces," *Proc. R. Soc. A*, 462, pp. 769-788.
- [24] Reddyhoff, T., Dwyer-Joyce, R. S., and Harper, P., 2008, "A New Approach for the Measurement of Film Thickness in Liquid Face Seals," *Tribology Transactions*, 51(2), pp. 140 - 149.
- [25] Zhang, J, Drinkwater, B.W., and Dwyer-Joyce, R.S., 2005, "Acoustic Measurement of Lubricant Film Thickness Distribution in Ball Bearings," *The Journal of the Acoustical Society of America*, 119(2), pp. 863-871.
- [26] Dwyer-Joyce, R. S., Drinkwater, B.W., and Donohoe, C.J., 2003, "The Measurement of Lubricant Film Thickness Using Ultrasound," *Proc. R. Soc. A*, 459, pp. 957-976.
- [27] Takeuchi, A., 2009, "Observation of lubrication conditions using an ultrasonic technique," *Lubrication Science*, 21, pp. 397-413.
- [28] Haines, N. F., 1980, "The Theory of Sound Transmission and Reflection at Contacting Surfaces," *C.E.G.B.*, Report No. RD/B/N4744.
- [29] Wooldridge, A. B., 1979, "The Effects of Compressive Stress on the Ultrasonic Response of Steel-Steel Interfaces and of Fatigue Cracks," *C.E.G.B.*, Report No. NW/SSD/RR/42/79.
- [30] Rokhlin, S. I., and Wang, L., 2002, "Ultrasonic Waves in Layered Anisotropic Media: Characterization of Multidirectional Composites," *International Journal of Solids and Structures*, 39(16), pp. 4133-4149.
- [31] Pau, M., Aymerich, F., Ginesu, F., 2001, "Measurements of nominal contact area in metallic surfaces: a comparison between an ultrasonic method and a pressure sensitive film," *Wear*, 249, pp. 533-535.
- [32] Dwyer-Joyce, R.S., and Drinkwater, B.W., 2004, "In-Situ Measurement of Contact Area and Pressure Distribution in Machine Elements," *Tribology Letters*, 14(1), pp. 41-52.
- [33] Tattersall, H.G., 1973, "The Ultrasonic Pulse-Echo Technique as Applied to Adhesion Testing," *Journal of Physics D: Applied Physics*, 6(7), pp. 819-832.
- [34] Thomas, T. R., and Sayles, R.S., 1977, "Stiffness of Machine Tool Joints: a Random-process Approach," *Trans. ASME: J. Engne Indust*, Paper no. 76-WA/Prod-23.
- [35] Dwyer-Joyce, R. S., Reddyhoff, T., and Drinkwater, B. W., 2004, "Operating Limits for Acoustic Measurement of Rolling Bearing Oil Film Thickness," *Tribology Transactions*, 47(3), pp. 366-375.
- [36] Rokhlin, S. I., and Wang, Y. J., 1991, "Analysis of Boundary Conditions for Elastic Wave Interaction with an Interface Between Two Solids," *J. Acoust. Soc. Am.*, 89, pp.503-515.
- [37] Hosten B., 1991, "Bulk Heterogeneous Plane-Wave Propagation Through Viscoelastic Plates and Stratified Media With Large Values of Frequency-Domain," *Ultrasonics*, 29 pp.445-50.
- [38] Silk, M.G., 1984, *Ultrasonic Transducers for Nondestructive Testing*, Adam Hilger, Bristol.
- [39] Greenwood, J. A., and Williamson, J. B. P., 1966, "Contact of Nominally Flat Surfaces," *Proc. R. Soc. A*, 295, pp. 300-319.
- [40] Onions, R. A., and Archard, J. F., 1973, "The Contact of Surfaces Having a Random Structure," *J Phys. D: Appf. Phys.*, pp. 289-304.
- [41] Whitehouse, D. J., and Archard, J. F., 1970, "The Properties of Random Surfaces of Significance in Their Contact," *Proc. R. Soc. A*, 316, pp. 97-121.
- [42] Bush, A. W., Gibson, R. D., and Thomas, T. R., 1975, "The Elastic Contact of a Rough Surface," *Wear*, 35, pp. 87-113.
- [43] Jacobson, B.O., and Vinet, P., 1987, "A Model for The Influence of Pressure on The Bulk Modulus and the Influence of Temperature on the Solidification Pressure of Liquid Lubricants," *ASME J. Tribol.*, 109, pp.709-715.
- [44] Jacobson, B.O., 2005, "High-pressure Chamber Measurements," *Proc. Inst. Mech. Eng. Part J: J. Eng. Tribol.*, 220, pp. 199-206.

Corresponding author: Juanjuan ZHU, Paper No: TRIB-10-1223, page number 24

- [45] Kondo, S., Sayles, S.R., and Lowe, M.J.S., 2006, "A Combined Optical-Ultrasonic Method of Establishing the Compressibility of High-Pressure Oil and Grease Films Entrapped in a Ball on Flat Contact," *Journal of Tribology*, 128(1), pp. 155-167.
- [46] Bair, S., 2007, *High Pressure Rheology for Quantitative Elastohydrodynamics*, Elsevier, Oxford, pp. 54-71.
- [47] Fakhreddine, Y.A., and Zoller, P., 1990, "The Equation of State of a Polydimethylsiloxane Fluid," *J. Appl. Polym. Sci.*, 41, pp. 1087-1093.
- [48] Hirschfelder, J.O., Curtiss, C.F., and Bird, R.B., 1954, *Molecular theory of Gases and Liquids*, Wiley, New York, pp.261.
- [49] Millat, J., Dymond, J.H., and de Castro, C.A.N., 1996, *Transport Properties of Fluids Their Correlation, Prediction and Estimation*, IUPAC, Cambridge, pp. 172.
- [50] Cook, R.L., King, H.E., Herbst, C.A., and Herschbach, D.R., 1994, "Pressure and Temperature Dependent Viscosity of Two Glass Forming Liquids: Glycerol and Dibutyl Phthalate," *J. Chem. Phys.*, 100(7), pp. 5178-5189.
- [51] Lu, X., Khonsari, M.M., Gelinck, E.R.M., 2006, "The Stribeck Curve: Experimental Results and Theoretical Prediction," *ASME J. Tribol.*, 126, pp. 789-794.
- [52] Hamrock, B. J., and Dowson, D., 1976, "Isothermal Elastohydrodynamic Lubrication of Point Contacts. I - Theoretical Formulation," *J. Lubr. Technol.*, 98(2), pp. 223-229.
- [53] Hamrock, B. J., and Dowson, D., 1977, "Isothermal Elastohydrodynamic Lubrication of Point Contacts. iii - Fully Flooded Results," *J. Lubr. Technol.*, 99(2), pp. 264-276.
- [54] Thomas, T.R., 1998, *Rough Surfaces*, Imperial College Press, London.